

## Functional and Mechanistic Analyses of Biomimetic Aminoacyl Transfer Reactions in de Novo Designed Coiled Coil Peptides via Rational Active Site Engineering

Luke J. Leman, Dana A. Weinberger, Zheng-Zheng Huang, Keith M. Wilcoxon, and M. Reza Ghadiri\*

Contribution from the Department of Chemistry and The Skaggs Institute for Chemical Biology, The Scripps Research Institute, 10550 North Torrey Pines Road, La Jolla, California 92037

Received November 10, 2006; E-mail: ghadiri@scripps.edu

**Abstract:** Ribosomes and nonribosomal peptide synthetases (NRPSs) carry out instructed peptide synthesis through a series of directed intermodular aminoacyl transfer reactions. We recently reported the design of coiled-coil assemblies that could functionally mimic the elementary aminoacyl loading and intermodular aminoacyl transfer steps of NRPSs. These peptides were designed initially to accelerate aminoacyl transfer mainly through catalysis by approximation by closely juxtaposing four active site moieties, two each from adjacent noncovalently associated helical modules. In our designs peptide self-assembly positions a cysteine residue that is used to covalently capture substrates from solution via transthioesterification (substrate loading step to generate the aminoacyl donor site) adjacent to an aminoacyl acceptor site provided by a covalently tethered amino acid or modeled by the  $\epsilon$ -amine of an active site lysine. However, through systematic functional analyses of 48 rationally designed peptide sequences, we have now determined that the substrate loading and intermodular aminoacyl transfer steps can be significantly influenced (up to  $\sim 10^3$ -fold) by engineering changes in the active site microenvironment through amino acid substitutions and variations in the inter-residue distances and geometry. Mechanistic studies based on  $^{15}\text{N}$  NMR and kinetic analysis further indicate that certain active site constellations furnish an unexpectedly large  $\text{p}K_{\text{a}}$  depression (1.5 pH units) of the aminoacyl-acceptor moiety, helping to explain the observed high rates of aminoacyl transfer in those constructs. Taken together, our studies demonstrate the feasibility of engineering efficient de novo peptide sequences possessing active sites and functions reminiscent of those in natural enzymes.

### Introduction

The wide breadth of reactions catalyzed by enzymes derives in large part from Nature's ability to form structurally precise, chemically tuned constellations of functional groups known as active sites. Among the numerous avenues that enzymes navigate to achieve rate enhancements, the most common features are (i) substrate binding events that lower entropic barriers, in part by bringing reactant molecules into close proximity and excluding bulk water molecules from the active site; (ii) precise spatial positioning of active site functional groups, providing for cooperative covalent or general acid/base catalysis, stabilization of transition state geometries, and specificity; and (iii) active site electrostatic optimization, including the dispersion of charge and  $\text{p}K_{\text{a}}$  perturbations of active site residues.<sup>1</sup> Clearly, designers of synthetic enzymes must likewise be able to predictably position and modulate the reactivity of active site residues if enzyme-like rates and specificity are to be realized.

Despite recent advances in the understanding of protein structure and function, the rational design of highly efficient peptide-based enzyme mimetics has remained elusive.<sup>2</sup> Furthermore, only a few examples are known that exploit perturbations of the reactivity of individual residues to enhance catalytic efficiencies. An early example was that of Benner and co-workers, whose synthetic helical peptides exploited  $\text{p}K_{\text{a}}$  depressions of amines from lysine side chains or the N-terminus to catalyze oxaloacetate decarboxylation with high efficiency.<sup>3</sup> The laboratories of Baltzer, Miller, and others have employed histidine sites on peptide scaffolds to catalyze acylation or *p*-nitrophenyl ester hydrolysis reactions with good efficiencies;<sup>4</sup> in several such designs,  $\text{p}K_{\text{a}}$  modulations of His residues were

(1) (a) Jencks, W. P. *Catalysis in Chemistry and Enzymology*, McGraw-Hill Series in Advanced Chemistry; McGraw-Hill Book Company: New York, 1969. (b) Fersht, A. *Structure and Mechanism in Protein Science*; W. H. Freeman and Company: U.S.A., 1999. (c) Wolfenden, R.; Snider, M. J. *Acc. Chem. Res.* **2001**, *34*, 938–45. (d) Bruice, T. C. *Acc. Chem. Res.* **2002**, *35*, 139–48. (e) Menger, F. M. *Pure Appl. Chem.* **2005**, *77*, 1873–86.

(2) Corey, M. J.; Corey, E. *Proc. Natl. Acad. Sci. U.S.A.* **1996**, *93*, 11428–34. (3) Johnson, K.; Allemann, R. K.; Widmer, H.; Benner, S. A. *Nature* **1993**, *365*, 530–2. (4) (a) Broo, K.; Brive, L.; Lundh, A. C.; Ahlberg, P.; Baltzer, L. *J. Am. Chem. Soc.* **1996**, *118*, 8172–3. (b) Broo, K.; Allert, M.; Andersson, L.; Erlandsson, P.; Stenhagen, G.; Wigstrom, J.; Ahlberg, P.; Baltzer, L. *J. Chem. Soc., Perkin Trans. 2* **1997**, *2*, 397–8. (c) Broo, K. S.; Brive, L.; Ahlberg, P.; Baltzer, L. *J. Am. Chem. Soc.* **1997**, *119*, 11362–72. (d) Broo, K. S.; Nilsson, H.; Nilsson, J.; Baltzer, L. *J. Am. Chem. Soc.* **1998**, *120*, 10287–95. (e) Jarvo, E. R.; Copeland, G. T.; Papaioannou, N.; Bonitatebus, P. J., Jr.; Miller, S. J. *J. Am. Chem. Soc.* **1999**, *121*, 11638–43. (f) Baltzer, L.; Nilsson, H.; Nilsson, J. *Chem. Rev.* **2001**, *101*, 3153–63. (g) Miller, S. J. *Acc. Chem. Res.* **2004**, *37*, 601–10. (h) Nicoll, A. J.; Allemann, R. K. *Org. Biomol. Chem.* **2004**, *2*, 2175–80. (i) Blank, J. T.; Miller, S. J. *Biopolymers* **2006**, *84*, 38–47.

suggested to promote catalysis. Further, positioning lysine residues within the hydrophobic core of four-helix bundle peptides has been shown to afford site selective Lys acylation stemming from side chain  $pK_a$  depressions of up to one  $pK$  unit.<sup>5</sup> Our group and others have demonstrated bimolecular peptide ligation reactions with efficiencies ( $[k_{cat}/K_M]/k_{uncat}$ ) of up to 5 orders of magnitude,<sup>6</sup> but in contrast to the designs described above, nearly all the observed rate enhancement in these ligases derived from entropic templating effects. Other examples of designed enzyme mimetics have employed prosthetic cofactors such as metal ions, porphyrins, flavins, hemes, or pyridoxamines in peptide-based scaffolds,<sup>7</sup> although in many cases the resulting reactivity was not appreciably different from the isolated prosthetic group.

Nonribosomal peptide synthetases (NRPSs)<sup>8</sup> generate peptide sequences by first loading amino acid substrates from solution onto carrier domains as aminoacyl thioesters and subsequently catalyzing directed intermodular aminoacyl transfer (Figure 1a). The present study focuses on the composite active sites located at the helical interfaces of recently designed coiled-coil peptides (Figure 2)<sup>9</sup> designed to mimic the two main steps of NRPS (aminoacyl loading and intermodular acyl transfer) by noncovalently assembling aminoacyl donor and acceptor modules into productive supramolecular complexes (Figures 1b, 2).<sup>9</sup> In our designs peptide self-assembly positions a cysteine residue, used for the covalent capture of substrates from solution via trans-thioesterification (substrate loading step to generate the aminoacyl donor site), adjacent to an aminoacyl acceptor site

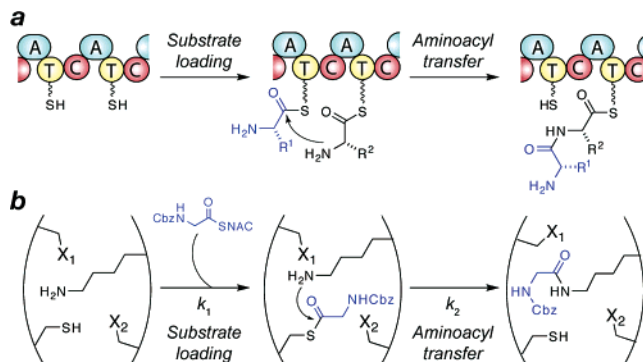


**Figure 1.** Schematic representation of aminoacyl substrate loading and intermodular aminoacyl transfer reactions in (a) nonribosomal peptide synthetases (NRPSs) and (b) the supramolecular peptides described here. A = adenylation domain, T = thiolation domain, C = condensation domain, SNAC = *N*-acetylcysteamine.

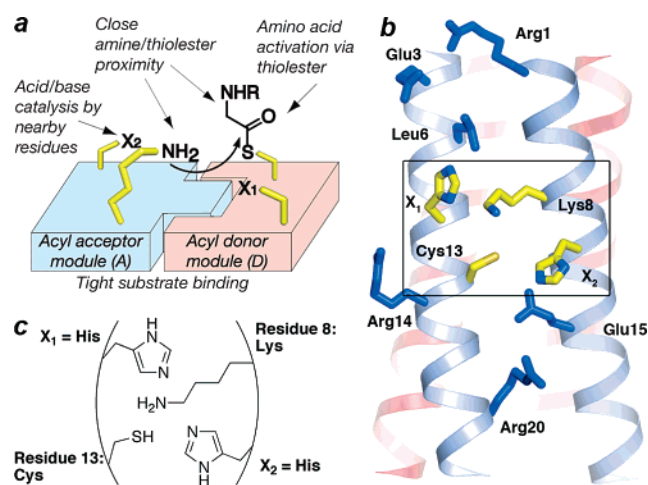


**Figure 2.** Representations of the composite aminoacyl transfer active sites. (a) Schematic diagram illustrating important principles of the active site design. (b) The positions of active site residues (yellow sticks, boxed) and secondary sphere residues (blue sticks) for sequence **1** are modeled onto the crystal structure<sup>12</sup> of a homotetrameric coiled-coil scaffold. For clarity, residues on only one of the four symmetry-related interhelical faces are shown. (c) Simplified active site representation for peptide **1**.

provided by a covalently tethered amino acid or the  $\epsilon$ -amine of an active site lysine (Figure 1b). The resulting high effective concentration of aminoacyl donor and acceptor moieties,<sup>10</sup> as well as the potential electrostatic and/or general acid/base contributions provided by the flanking  $X_1$  and  $X_2$  residues, were expected to afford significant intermodular aminoacyl transfer rate accelerations. In the present study, we have systematically varied the inter-residue distances, identities, and positions of active site residues using 48 rationally designed peptide sequences (Table 1) to probe the influence of active site microenvironments on the overall catalytic efficiency. We demonstrate that the substrate loading and intermodular ami-

- (5) (a) Allert, M.; Baltzer, L. *Chem.—Eur. J.* **2002**, *8*, 2549–60. (b) Andersson, L. K.; Caspersson, M.; Baltzer, L. *Chem.—Eur. J.* **2002**, *8*, 3687–97.
- (6) (a) Lee, D. H.; Granja, J. R.; Martinez, J. A.; Severin, K.; Ghadiri, M. R. *Nature* **1996**, *382*, 525–8. (b) Severin, K.; Lee, D. H.; Martinez, J. A.; Ghadiri, M. R. *Chem.—Eur. J.* **1997**, *3*, 1017–24. (c) Severin, K.; Lee, D. H.; Kennan, A. J.; Ghadiri, M. R. *Nature* **1997**, *389*, 706–9. (d) Yao, S.; Ghosh, I.; Zutshi, R.; Chmielewski, J. *J. Am. Chem. Soc.* **1997**, *119*, 10559–60. (e) Yao, S.; Ghosh, I.; Zutshi, R.; Chmielewski, J. *Nature* **1998**, *396*, 447–50. (f) Kennan, A. J.; Haridas, V.; Severin, K.; Lee, D. H.; Ghadiri, M. R. *J. Am. Chem. Soc.* **2001**, *123*, 1797–803. (g) Matsumura, S.; Takahashi, T.; Ueno, A.; Mihara, H. *Chem.—Eur. J.* **2003**, *9*, 4829–37.
- (7) (a) Sasaki, T.; Kaiser, E. T. *J. Am. Chem. Soc.* **1989**, *111*, 380–1. (b) Mihara, H.; Tomizaki, K. Y.; Nishino, N.; Fujimoto, T. *Chem. Lett.* **1993**, 1533–6. (c) Choma, C. T.; Lear, J. D.; Nelson, M. J.; Dutton, P. L.; Robertson, D. E.; DeGrado, W. F. *J. Am. Chem. Soc.* **1994**, *116*, 856–65. (d) Geier, G. R.; Sasaki, T. *Peptides: Chemistry, Structure and Biology, Proceedings of the American Peptide Symposium, 14th, Columbus, Ohio, June 18–23, 1995* **1996**, 591–2. (e) Roy, R. S.; Imperiali, B. *Protein Eng.* **1997**, *10*, 691–8. (f) Sakamoto, S.; Ueno, A.; Mihara, H. *J. Chem. Soc., Perkin Trans. 2* **1998**, 2395–404. (g) Baltzer, L. *Curr. Opin. Struct. Biol.* **1998**, *8*, 466–70. (h) Shogren-Knaak, M. A.; Imperiali, B. *Bioorg. Med. Chem.* **1999**, *7*, 1993–2002. (i) Geier, G. R., III; Sasaki, T. *Tetrahedron* **1999**, *55*, 1859–70. (j) Tomizaki, K.; Tsunekawa, Y.; Akisada, H.; Mihara, H.; Nishino, N. *J. Chem. Soc., Perkin Trans. 2* **2000**, *4*, 813–22. (k) Lombardi, A.; Nastro, F.; Pavone, V. *Chem. Rev.* **2001**, *101*, 3165–89. (l) Rosenblatt, M. M.; Wang, J.; Suslick, K. S. *Proc. Natl. Acad. Sci. U.S.A.* **2003**, *100*, 13140–5. (m) Kaplan, J.; DeGrado, W. F. *Proc. Natl. Acad. Sci. U.S.A.* **2004**, *101*, 11566–70. (n) Sakamoto, S.; Ito, A.; Kudo, K.; Yoshikawa, S. *Chem.—Eur. J.* **2004**, *10*, 3717–26. (o) Butterfield, S. M.; Goodman, C. M.; Rotello, V. M.; Waters, M. L. *Angew. Chem., Int. Ed.* **2004**, *43*, 724–7. (p) Huang, S. S.; Koder, R. L.; Lewis, M.; Wand, A. J.; Dutton, P. L. *Proc. Natl. Acad. Sci. U.S.A.* **2004**, *101*, 5536–41. (q) Ishida, M.; Dohmae, N.; Shiro, Y.; Oku, T.; Iizuka, T.; Isogai, Y. *Biochemistry* **2004**, *43*, 9823–33. (r) Zhuang, J.; Amoroso, J. H.; Kinloch, R.; Dawson, J. H.; Baldwin, M. J.; Gibney, B. R. *Inorg. Chem.* **2004**, *43*, 8218–20. (s) Rossi, P.; Tecilla, P.; Baltzer, L.; Scrimin, P. *Chem.—Eur. J.* **2004**, *10*, 4163–70. (t) Nanda, V.; Rosenblatt, M. M.; Osyczka, A.; Kono, H.; Getahun, Z.; Dutton, P. L.; Saven, J. G.; DeGrado, W. F. *J. Am. Chem. Soc.* **2005**, *127*, 5804–5. (u) Cochran, F. V.; Wu, S. P.; Wang, W.; Nanda, V.; Saven, J. G.; Therien, M. J.; DeGrado, W. F. *J. Am. Chem. Soc.* **2005**, *127*, 1346–7. (v) Fukushima, H.; Sakamoto, S.; Kudo, K. *Pept. Sci.* **2006**, *42*, 419–22.
- (8) (a) Cane, D. E.; Walsh, C. T. *Chem. Biol.* **1999**, *6*, R319–R25. (b) Khosla, C.; Harbury, P. B. *Nature* **2001**, *409*, 247–52. (c) Sieber, S. A.; Marahiel, M. A. *Chem. Rev.* **2005**, *105*, 715–38. (d) Fischbach, M. A.; Walsh, C. T. *Chem. Rev.* **2006**, *106*, 3468–96.
- (9) Wilcoxen, K. M.; Leman, L. J.; Weinberger, D. A.; Huang, Z.-Z.; Ghadiri, M. R. *J. Am. Chem. Soc.* **2007**, *129*, 748–9.

- (10) (a) Wieland, T.; Bokelmann, E.; Bauer, L.; Lang, H. U.; Lau, H.; Schafer, W. *Justus Liebigs Ann. Chem.* **1953**, 583, 129–49. (b) Brenner, M. *Pept. Proc. Eur. Pept. Symp.*, *8th* **1967**, 1–7. (c) Neumann, H.; Shashoua, V. E.; Sheehan, J. C.; Rich, A. *Proc. Natl. Acad. Sci. U.S.A.* **1968**, *61*, 1207–14. (d) Kemp, D. S. *Biopolymers* **1981**, *20*, 1793–804. (e) Sasaki, S.; Shionoya, M.; Koga, K. *J. Am. Chem. Soc.* **1985**, *107*, 3371–2. (f) Dawson, P. E.; Muir, T. W.; Clark-Lewis, I.; Kent, S. B. H. *Science* **1994**, *266*, 776–9. (g) Tamura, K.; Schimmel, P. *Proc. Natl. Acad. Sci. U.S.A.* **2001**, *98*, 1393–7. (h) Offer, J.; Boddy, C. N. C.; Dawson, P. E. *J. Am. Chem. Soc.* **2002**, *124*, 4642–6. (i) Leleu, S.; Penhoat, M.; Bouet, A.; Dupas, G.; Papamicael, C.; Marsais, F.; Levacher, V. *J. Am. Chem. Soc.* **2005**, *127*, 15668–9. (j) Snyder, T. M.; Liu, D. R. *Angew. Chem., Int. Ed.* **2005**, *44*, 7379–82. (k) Chen, G.; Warren, J. D.; Chen, J.; Wu, B.; Wan, Q.; Danishefsky, S. J. *J. Am. Chem. Soc.* **2006**, *128*, 7460–2.

**Table 1.** Active Sites, Molar Ellipticities, and Sequences of the Designed Peptides<sup>a</sup>

peptide	residue 8	residue 13	X <sub>1</sub>	X <sub>2</sub>	N <sub>agg</sub>	[ $\theta$ ] (deg cm <sup>2</sup> dmol <sup>-1</sup> )	sequence
1	Lys	Cys	His	His	4	-25 800	Aba-RLENILSKLHHICRELARIRLLGER-CONH <sub>2</sub>
1*	Lys	Cys	His	His	4	-23 200	Aba-RRLENILSKLHHI(C <sup>Ac</sup> m)RELARIRLLGERRR-CONH <sub>2</sub>
2	Orn	Cys	His	His	4	-24 500	Aba-RLENILS(Orn)LHHICRELARIKLLGER-CONH <sub>2</sub>
3	Lys	HCys	His	His	4	-25 200	Aba-RLENILSKLHHI(HCys)RELARIKLLGER-CONH <sub>2</sub>
4	Orn	HCys	His	His	4	-24 700	Aba-RLENILS(Orn)LHHI(HCys)RELARIKLLGER-CONH <sub>2</sub>
5	Lys	Cys	His	His	4	-28 400	Aba-RMKQIEDKLENILSKLHHICRELARIKLLGER-CONH <sub>2</sub>
6	Lys	Cys	His	His	3	-27 600	Aba-RMKQIEDKLENILSKIHHCREIARIKLLGER-CONH <sub>2</sub>
7	Lys	Cys	His	His	2	-27 000	Aba-RMKQLEDKLENILSKIHHLKREIARLKKLIGER-CONH <sub>2</sub>
8	Cys	Lys	His	His	4	-30 400	Aba-RMKQIEDKLENILSCLHHIKRELARIKLLGER-CONH <sub>2</sub>
9	Cys	Lys	His	His	3	-24 100	Aba-RMKQIEDKLENILSCIHHIKREIARIKLLGER-CONH <sub>2</sub>
10	Cys	Lys	His	His	2	-25 700	Aba-RMKQLEDKLENILSCLHHIKREIARLKKLIGER-CONH <sub>2</sub>
11	Lys	Cys	Arg	Arg	4	-22 900	Aba-RLENILSKLRRICRELARIRLLGER-CONH <sub>2</sub>
12	Lys	Cys	Phe	Phe	4	-26 000	Aba-RLENILSKLFFICRELARIRLLGER-CONH <sub>2</sub>
13	Lys	Cys	Asn	Asn	4	-24 500	Aba-RLENILSKLNNICRELARIRLLGER-CONH <sub>2</sub>
14	Lys	Cys	Ala	Ala	4	-25 200	Aba-RLENILSKLAAICRELARIKLLGER-CONH <sub>2</sub>
14*	Lys	Cys	Ala	Ala	4	-25 600	Aba-RRLENILSKLAAI(C <sup>Ac</sup> m)RELARIRLLGERRR-CONH <sub>2</sub>
15	Lys	Cys	Asp	Asp	4	-27 300	Aba-RLENILSKLDDICRELARIRLLGER-CONH <sub>2</sub>
15*	Lys	Cys	Asp	Asp	4	-28 000	Aba-RRLENILSKLDDI(C <sup>Ac</sup> m)RELARIRLLGERRR-CONH <sub>2</sub>
16	Lys	Cys	Arg	His	4	-26 300	Aba-RLENILSKLRHICRELARIRLLGER-CONH <sub>2</sub>
17	Lys	Cys	Phe	His	4	-24 900	Aba-RLENILSKLFHICRELARIRLLGER-CONH <sub>2</sub>
18	Lys	Cys	Asn	His	4	-24 900	Aba-RLENILSKLNHICRELARIRLLGER-CONH <sub>2</sub>
19	Lys	Cys	Ala	His	4	-24 300	Aba-RLENILSKLAHICRELARIKLLGER-CONH <sub>2</sub>
20	Lys	Cys	Asp	His	4	-26 000	Aba-RLENILSKLDHICRELARIKLLGER-CONH <sub>2</sub>
21	Lys	Cys	His	Arg	4	-22 800	Aba-RLENILSKLHRICRELARIRLLGER-CONH <sub>2</sub>
22	Lys	Cys	His	Phe	4	-24 500	Aba-RLENILSKLHFICRELARIRLLGER-CONH <sub>2</sub>
23	Lys	Cys	His	Ala	4	-23 100	Aba-RLENILSKLHAICRELARIKLLGER-CONH <sub>2</sub>
24	Lys	Cys	His	Asp	4	-25 500	Aba-RLENILSKLHDICRELARIRLLGER-CONH <sub>2</sub>
25	Cys	Lys	His	His	4	-26 400	Aba-RLENILSCLHHIKRELARIKLLGER-CONH <sub>2</sub>
25*	Cys	Lys	His	His	4	-23 100	Aba-RRLENILS(C <sup>Ac</sup> m)LHHIKRELARIRLLGERRR-CONH <sub>2</sub>
26	Cys	Lys	Ala	Ala	4	N.D.	Aba-RLENILSCLAAIKRELARIRLLGER-CONH <sub>2</sub>
27	Cys	Lys	Ala	His	4	N.D.	Aba-RLENILSCLAHIKRELARIRLLGER-CONH <sub>2</sub>
28	Cys	Lys	Asp	His	4	N.D.	Aba-RLENILSCLDHIKRELARIRLLGER-CONH <sub>2</sub>
29	Cys	Lys	His	Ala	4	N.D.	Aba-RLENILSCLHAIKRELARIRLLGER-CONH <sub>2</sub>
30	Cys	Lys	His	Asp	4	N.D.	Aba-RLENILSCLHDIKRELARIRLLGER-CONH <sub>2</sub>
31	Cys	Cys	His	His	4	N.D.	Aba-RLENILSCLHHICRELARIRLLGER-CONH <sub>2</sub>
32	Cys	Cys	His	Asp	4	N.D.	Aba-RLENILSCLHDICRELARIRLLGER-CONH <sub>2</sub>
33	Cys	Cys	Asp	His	4	N.D.	Aba-RLENILSCLDHICRELARIRLLGER-CONH <sub>2</sub>
34	Lys	Ser	His	His	4	-25 000	Aba-RLENILSKLHHISRELARIRLLGER-CONH <sub>2</sub>
35	Lys	Ser	Ala	His	4	-25 800	Aba-RLENILSKLAHISRELARIRLLGER-CONH <sub>2</sub>
36	Tripeptide		~	~	~	N.D.	Aba-SKL-COOH
37	Lys	Ser	His	His	4	N.D.	Aba-RLENILSKLHHISRELARIRLLGER-CONH <sub>2</sub>
38	Lys	Cys	His	His	4	-27 300	Aba-RLENILSKLHHICSRARIRLLGER-CONH <sub>2</sub>
39	Lys	Cys	His	His	4	-25 600	Aba-ELANIRSKLHHICSRARIRLLGER-CONH <sub>2</sub>
40	Cys	Lys	His	His	4	-27 100	Aba-RLENILSCLHHIKSRARIRLLGER-CONH <sub>2</sub>
41	Cys	Lys	His	His	4	-25 000	Aba-ELANIRSKLHHIKSRARIRLLGER-CONH <sub>2</sub>
42	Lys	Cys	His	Ala	4	-27 800	Aba-RLENILSKLHAICSRARIRLLGER-CONH <sub>2</sub>
43	Lys	Cys	His	His	4	-31 200	Aba-AMRQIRDELANIRSKLHHICSRARIRLLGER-CONH <sub>2</sub>
44	Cys	Lys	His	His	4	-30 900	Aba-AMRQIRDELANIRSKLHHIKSRARIRLLGER-CONH <sub>2</sub>

<sup>a</sup> Molar ellipticity values were recorded at 222 nm for peptides (20  $\mu$ M) in pH 7.0 MOPS buffer (10 mM). N.D. = not determined. (C<sup>Ac</sup>m) denotes acetamidomethyl-protected Cys residue, (Orn) denotes ornithine, and (HCys) denotes homocysteine. N<sub>agg</sub> denotes coiled-coil aggregation state as specified by the nature of the hydrophobic core residues present.<sup>11</sup>

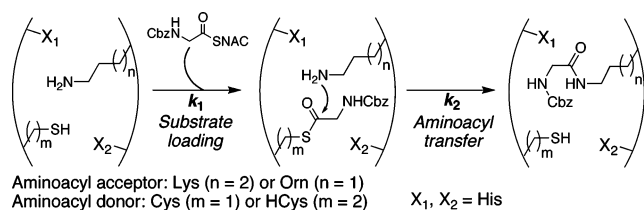
noacyl transfer steps can be significantly influenced (up to  $\sim 10^3$ -fold) by engineering changes in the active site microenvironment.

## Results and Discussion

**Effect of Relative Distance and Orientation of Aminoacyl-Donor and -Acceptor Sites.** According to our design rationale, catalysis by approximation was expected to be the primary factor in accelerating the rates of intermodular aminoacyl transfer. Accordingly, we sought to examine the effect of changes in the relative orientation and distances between the aminoacyl-donor and -acceptor moieties on the overall reaction efficiency. We prepared peptides 2–4 (Table 2) in which ornithine (one methylene group shorter than Lys) and homocysteine (one methylene group longer than Cys) were substituted for the acyl-acceptor and -donor groups in peptide 1, respectively.<sup>9</sup> While

substrate loading rates ( $k_1$ ) were largely unaffected, the presence of these residues in all cases decreased the aminoacyl transfer rates ( $k_1$ ) by 5- to 8-fold (Table 2), suggesting that small changes to active site inter-residue distances can appreciably alter aminoacyl transfer efficiency. An alternative approach to varying active site inter-residue distances and geometries is through modifying the coiled-coil scaffold aggregation state (sequences 5–10). As a result of the hydrophobic core expansion and the accompanying changes in relative helix–helix rotation in going from dimeric to tetrameric assemblies, the relative active site side chain  $\alpha$ – $\beta$ -carbon atom vectors are altered and the interhelical active site distances are shortened and more buried at the interface (Figure 3).<sup>11</sup> Peptides 7 and 10 designed to form dimeric bundles (as specified by Ile and Leu residues in the *a*

(11) Harbury, P. B.; Zhang, T.; Kim, P. S.; Alber, T. *Science* 1993, 262, 1401–7.

**Table 2.** Effect of Active Site Inter-residue Distances on Aminoacyl Loading and Transfer Rates

peptide	residue 8 <sup>b</sup>	residue 13 <sup>b</sup>	$N_{\text{agg}}^c$	$k_1$ ( $10^{-3} \text{ s}^{-1}$ )	$k_2$ ( $10^{-4} \text{ s}^{-1}$ )
26 residue peptides:					
1	Lys	Cys	4	1.3	9.2
2	Orn	Cys	4	2.1	1.2
3	Lys	HCys	4	0.9	1.7
4	Orn	HCys	4	0.9	1.2
33 residue peptides:					
5	Lys	Cys	4	0.8	2.9
6	Lys	Cys	3	2.7	1.4
7	Lys	Cys	2	3.0	0.4
8	Cys	Lys	4	0.3	0.8
9	Cys	Lys	3	2.1	2.0
10	Cys	Lys	2	> 10	0.4

<sup>a</sup> Reactions contained  $\sim 100 \mu\text{M}$  peptide, 10 mM Cbz-Gly-SNAC substrate, 10 mM tris-carboxyethyl phosphine (TCEP) as reducing agent, 285 mM Hepes pH 7.0, and  $\sim 200 \mu\text{M}$  acetamidobenzoic acid (Aba) as internal concentration standard. Rate constants were determined from reaction modeling using SIMFIT.<sup>21</sup> See Table 1 for complete peptide sequences. <sup>b</sup> Orn denotes ornithine; HCys denotes homocysteine. In the 33-residue sequences, the “residue 8” and “residue 13” designations correspond to sequence positions 15 and 20 due to the seven additional N-terminal residues. <sup>c</sup>  $N_{\text{agg}}$  denotes coiled-coil aggregation state as specified by the nature of the hydrophobic core residues present.<sup>11</sup>

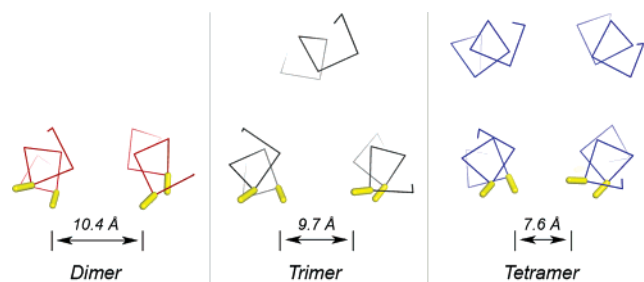


**Figure 3.** Structural consequences of varying the coiled-coil aggregation state on active site residues. Average interhelical distances between  $\beta$ -carbons of  $e$  and  $g$  heptad positions decrease from the dimeric to the tetrameric state. Further, active site side chains are projected more directly toward the adjacent helix in the higher aggregates, as indicated by an inspection of side chain  $\alpha \rightarrow \beta$ -carbon atom vectors (yellow sticks). Each assembly shown is the crystallographic structure of a GCN4-derived peptide.<sup>11,19</sup> The figure was generated using PYMOL.<sup>20</sup>

and  $d$  core positions, respectively<sup>11</sup>) had higher substrate loading rates than trimeric sequences **6** and **9** (Ile in core positions<sup>11</sup>) or tetrameric peptides **5** and **8** (Leu and Ile in the  $a$  and  $d$  core positions, respectively<sup>11</sup>). These results can be rationalized by considering that the bimolecular transthioesterification reaction is likely to proceed more efficiently with acyl-donor residues present at the more exposed helical interface in a dimeric assembly (Figure 2). On the other hand, the dimeric peptides exhibited marginally lower aminoacyl transfer rates than the higher aggregates (Table 2), likely due to the poorer proximity and less productive trajectories of the acyl-donor and -acceptor species relative to the tri- and tetrameric species. Varying inter-residue geometry can also be achieved by switching the position of the active site aminoacyl-donor and -acceptor residues.

Comparisons of the loading and transfer rate constants between peptides **5** and **8**, **6** and **9**, and **7** and **10** (Table 2) clearly indicate that only small differences ( $< 4$ -fold) result from switching the relative position of the active site acyl-acceptor and -donor moieties. Taken together, these studies indicate that modest alterations of active site inter-residue distances or the relative donor/acceptor positioning have a less than 10-fold impact on the observed rates of aminoacyl loading and transfer.

**Effects of Active Site Amino Acid Substitutions.** Analyses of the crystal structures of parallel tetrameric coiled-coil assemblies<sup>11–13</sup> indicated that the  $X_1$  and  $X_2$  amino acid residues (Figure 2) should be in close proximity to the active site aminoacyl donor and acceptor moieties and therefore could provide electrostatic contributions or general acid–base catalysis in the course of aminoacyl loading and transfer processes. Accordingly, we investigated a series of peptides with amino acid substitutions at the  $X_1$  and  $X_2$  active site positions (sequences **11–30**). These variants were designed to explore the contributions of hydrophobic, polar, or charged active site microenvironments to the aminoacyl loading and transfer rates. Interestingly, the apparent intermolecular aminoacyl transfer rate constants ( $k_2$ ) for these peptides varied by more than 200-fold (Table 3, Figure 4a), while substrate loading rates ( $k_1$ ) varied by  $\sim 20$ -fold. The most efficient sequences contained active site histidine, arginine, or phenylalanine residues (positively charged or hydrophobic microenvironments), while the least efficient aminoacyl loading and transfer in general occurred in the presence of active site aspartic acid residues (negatively charged microenvironments). Replacing either or both His residues at  $X_1$  or  $X_2$  positions with Ala resulted in transfer rate decreases of 7-fold (peptide **19**), 13-fold (peptide **23**), and 18-fold (peptide **14**) (Table 3). The active site His residues appear to behave cooperatively, as peptide **1** is more efficient than would be expected from summing the marginal rate improvements of the His/Ala and Ala/His sequences (peptides **23** and **19**) relative to the Ala/Ala peptide (sequence **14**).<sup>9</sup> The observed efficiency of aminoacyl transfer in sequences lacking active site histidines (peptides **11–14**) discounts the possibility of acylimidazole intermediates in the course of the reaction. Therefore, the observed rate accelerations in constructs with active site histidines are most likely due to general acid–base or proton-transfer catalysis. In the peptide variants that contain the aminoacyl-acceptor site at position 8 (sequences **1**, **11–24**), the  $X_1$  residue more significantly influences the efficiency of aminoacyl transfer than  $X_2$  (Figure 4a). For instance, the aminoacyl transfer rate ( $k_2$ ) for sequence **1** ( $X_1 = \text{His}$ ) decreased by  $> 30$ -fold when  $X_1$  site was substituted with Asp (peptide **20**), whereas Asp substitution at  $X_2$  (sequence **24**) reduced the rate by only 5-fold. In contrast, when the relative orientation of the active site aminoacyl-donor and -acceptor positions was switched (sequences **25–30**), amino acid substitutions at the  $X_2$  site were more influential (Table 3). The difference in aminoacyl transfer rate between sequence **25** ( $X_1 = \text{His}$ ) and the single  $X_1$  Asp substitution (peptide **28**) was just 3-fold, whereas the single  $X_2$  Asp substitution (sequences **30**) differed from **25** by 15-fold. Our studies indicate that the pronounced reductions in the rate of aminoacyl transfer in peptides bearing

(12) Yadav, M. K.; Redman, J. E.; Leman, L. J.; Alvarez-Gutierrez, J. M.; Zhang, Y.; Stout, C. D.; Ghadiri, M. R. *Biochemistry* **2005**, *44*, 9723–32.

(13) Yadav, M. K.; Leman, L. J.; Price, D. J.; Brooks, C. L.; Stout, C. D.; Ghadiri, M. R. *Biochemistry* **2006**, *45*, 4463–73.

**Table 3.** Effect of Active Site  $X_1$  and  $X_2$  Positions on Aminoacyl Loading and Transfer Rates<sup>a</sup>

**Peptides 1, 11 – 24**

**Peptides 25 – 30**

peptide	$X_1$	$X_2$	$k_1$ ( $10^{-3} \text{ s}^{-1}$ )	$k_2$ ( $10^{-4} \text{ s}^{-1}$ )
1	His	His	1.3	9.2
11	Arg	Arg	2.2	2.4
12	Phe	Phe	1.0	2.7
13	Asn	Asn	2.3	0.6
14	Ala	Ala	3.4	0.5
15	Asp	Asp	0.4	0.04
16	Arg	His	1.5	7.1
17	Phe	His	2.1	0.7
18	Asn	His	0.6	1.4
19	Ala	His	1.0	1.3
20	Asp	His	0.2	0.3
21	His	Arg	1.3	2.3
22	His	Phe	0.7	2.6
23	His	Ala	1.3	0.7
24	His	Asp	0.8	1.8
25	His	His	3.1	1.5
26	Ala	Ala	6.4	0.9
27	Ala	His	5.1	1.4
28	Asp	His	0.9	0.5
29	His	Ala	3.1	1.4
30	His	Asp	0.4	0.1

<sup>a</sup> Reaction conditions are as described in Table 2. See Table 1 for complete peptide sequences.

an active site aspartic acid residue(s) stem from electrostatic perturbations that significantly alter the  $pK_a$  of the acyl acceptor amine (vide infra).

#### Directed Intermodular Aminoacyl Transfer Reactions.

The above findings suggest that the judicious choice of amino acids at  $X_1$  and  $X_2$  positions could be exploited to bring about directed aminoacyl transfer by selectively increasing or decreasing transfer efficiency at particular positions. This possibility was explored using sequences **31–33** in which phenylalanyl thioesters preloaded on Cys residues at positions 8 and 13 were used as the active site aminoacyl-donor and -acceptor moieties (Table 4, Figure 4b). Unlike peptides containing an active site Lys as the aminoacyl acceptor moiety and an N-protected aminoacyl thioester as the donor, in sequences **31–33** aminoacyl transfer can proceed via two distinct pathways: with the thioester at position 8 acting as the acceptor and the thioester at position 13 acting as the donor, or vice versa. Interestingly, for sequences **31** and **32** ( $X_1 = \text{His}$ ) we observe only evidence of position 8 acting as the acyl-acceptor moiety (no dipeptide

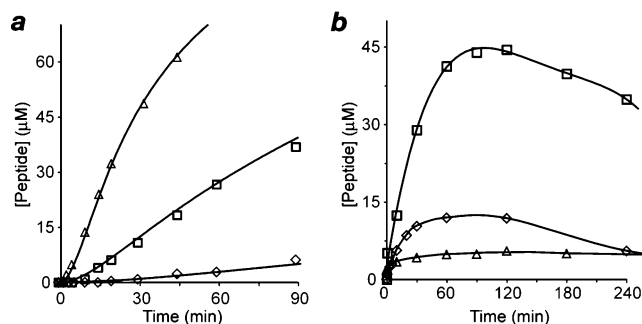


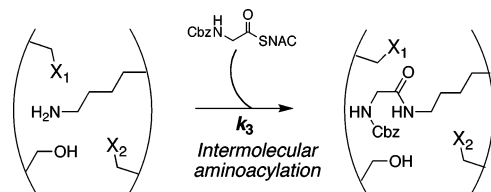
**Figure 4.** Effect of active site  $X_1$  and  $X_2$  residues on aminoacyl transfer efficiency. (a) Aminoacyl transfer product formation in time for peptides **1** ( $\Delta$ ,  $X_1 = \text{His}$ ), **19** ( $\square$ ,  $X_1 = \text{Ala}$ ), and **20** ( $\diamond$ ,  $X_1 = \text{Asp}$ ). Curve fits shown are from reaction modeling using SIMFIT.<sup>21</sup> (b) Formation of coiled-coil-bound dipeptide thioester species in time for sequences **31** ( $\diamond$ ,  $X_1 = \text{His}$ ,  $X_2 = \text{His}$ ), **32** ( $\square$ ,  $X_1 = \text{His}$ ,  $X_2 = \text{Asp}$ ), and **33** ( $\Delta$ ,  $X_1 = \text{Asp}$ ,  $X_2 = \text{His}$ ). For sequences **31** and **32** ( $X_1 = \text{His}$ ), all coiled-coil-bound dipeptide species were observed at Cys8, whereas, for sequence **33** ( $X_1 = \text{Asp}$ ), the coiled-coil-bound products were instead observed at Cys13 (as determined by comparison with authentic samples), suggesting that the  $X_1$  and  $X_2$  residues could be used to direct ordered peptide synthesis by modulating the relative transfer efficiencies of distinct aminoacyl thioesters anchored in the active site.

**Table 4.** Effect of Active Site  $X_1$  and  $X_2$  Positions on Relative Acyl-Donor and -Acceptor Reactivity in Active Sites Composed of Two Aminoacyl Thioester Moieties<sup>a</sup>

peptide	$X_1$	$X_2$	observed acceptor site <sup>b</sup>
31	His	His	Cys8
32	His	Asp	Cys8
33	Asp	His	Cys13

<sup>a</sup> Reaction conditions are as described in Table 2, without the addition of the Cbz-Gly-SNAC substrate. See Table 1 for complete peptide sequences. <sup>b</sup> Denotes observed site of coiled-coil-bound dipeptide thioester species (as determined by comparison with independently prepared authentic samples). For all peptides, coiled-coil-bound products were observed only at Cys8 or at Cys13 (not at both positions).

species are observed at position 13), whereas for sequence **33** ( $X_1 = \text{Asp}$ ) we instead observe only evidence of position 13 acting as the aminoacyl acceptor (Table 4, Figure 4b). These findings are consistent with the observed higher aminoacyl transfer rates for peptide **24** ( $X_1 = \text{His}$ ,  $X_2 = \text{Asp}$ , acceptor at position 8) than those for **30** ( $X_1 = \text{His}$ ,  $X_2 = \text{Asp}$ , acceptor at position 13) and the higher rate for **28** ( $X_1 = \text{Asp}$ ,  $X_2 = \text{His}$ , acceptor at position 13) than that for **20** ( $X_1 = \text{Asp}$ ,  $X_2 = \text{His}$ , acceptor at position 8) and support the suggestion that the  $X_1$

**Table 5.** Rates of Intermolecular Lys Aminoacylation


peptide	X <sub>1</sub>	X <sub>2</sub>	k <sub>3</sub> (10 <sup>-4</sup> s <sup>-1</sup> )
<b>34</b>	His	His	0.09
<b>35</b>	Ala	His	0.02
<b>36</b>	tripeptide; no active site		0.002
<b>37, Lys8</b>	His	His	0.09
<b>37, Lys21</b>	solvent-exposed; no active site		0.003

<sup>a</sup> Reaction conditions are as described in Table 2. See Table 1 for complete peptide sequences.

and X<sub>2</sub> active site positions may indeed be employed to foster directed aminoacyl transfer through selective active site microenvironment perturbations. It should be noted that the analysis of these reactions is complicated by substrate hydrolysis and cyclization (diketopiperazine formation) of the resulting dipeptide thiolester (Table 4). The apparent higher initial rate of aminoacyl transfer for sequence **32** (X<sub>2</sub> = Asp) than that for sequence **31** (X<sub>2</sub> = His) (Figure 4b) indeed results from its lower rate of diketopiperazine formation (data not shown).

**Active Site Dependent pK<sub>a</sub> Perturbations.** Control peptides **34** and **35** in which the active site Cys was substituted with Ser to prevent substrate loading were prepared for experiments aimed at estimating aminoacyl transfer rate enhancements. Interestingly, although as expected based on the design rationale the observed rates of intermolecular aminoacylation with these peptides were reduced by 100-fold with respect to parent peptide **1**, these rates were nevertheless faster by 10- to 45-fold as compared to the reference tripeptide **36** (Table 5).<sup>9</sup> To further investigate the source of this discrepancy, we prepared peptide **37** containing two Lys residues, one in the active site environment (again containing the Cys→Ser substitution to prevent aminoacyl loading) and one located at a solvent-exposed position near the peptide terminus (Figure 5a). Subjecting this peptide to standard reaction conditions indicated that the active site lysine underwent bimolecular aminoacylation 30-fold more efficiently than the solvent-exposed lysine (established via tryptic digestion and MS sequencing analysis) even though the terminal Lys21 is presumably more sterically accessible (Figure 5a, Table 5). We suspected that this anomalous reactivity might have resulted from pK<sub>a</sub> depression of the active-site Lys residue brought about by the active site microenvironment. Because direct measurements of pK<sub>a</sub> values of specific functional groups in proteins and peptides can be most accurately measured using NMR by monitoring the chemical shift of the desired nucleus as a function of pH,<sup>14</sup> we employed <sup>15</sup>N NMR to establish the role of pK<sub>a</sub> shifts in the efficiency of aminoacyl transfer reactions. The use of NMR circumvents potential problems

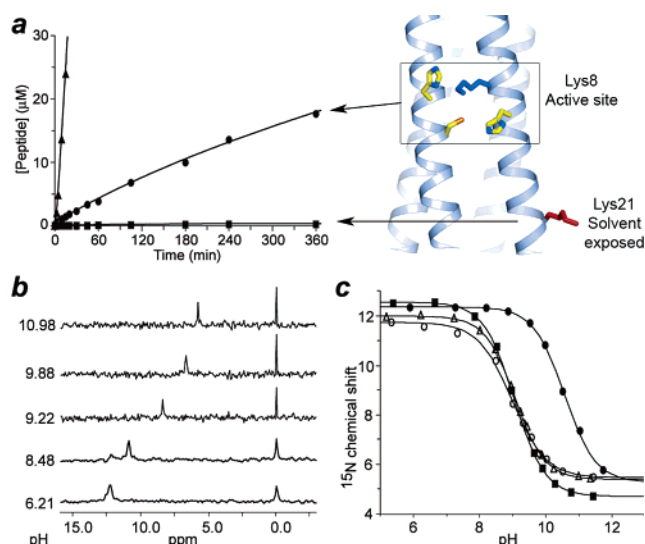


**Figure 5.** Enhanced aminoacyl acceptor reactivity in the designed active site. (a) Peptide **37** contains two lysine residues, one in the partially buried composite active site (Lys8, blue) and one at a C-terminal solvent-exposed position (Lys21, red). Even though substrate loading cannot occur due to an active site Cys→Ser substitution, the active site Lys8 (●) undergoes bimolecular aminoacylation by the Cbz-Gly-SNAC thiolester at a rate 30-fold higher than the more solvent-exposed Lys21 (■). A product formation curve is also shown for peptide **1** for comparison (▲). Curve fits shown are from reaction modeling using SIMFIT.<sup>21</sup> (b) Selected <sup>15</sup>N NMR spectra for peptide **1**\* for use in active site Lys pK<sub>a</sub> determination. At each pH value, 1200–4000 scans were recorded. The outer coaxial NMR tube (10 mm) contained peptide **1**\* (3 mM), acetate (6 mM), bis-tris (6 mM), and CAPS buffers (6 mM) in H<sub>2</sub>O, while the inner tube (3 mm) contained <sup>15</sup>N-labeled ammonium nitrate (<sup>15</sup>NH<sub>4</sub>NO<sub>3</sub>, 2.0 M) dissolved in 95% D<sub>2</sub>O for reference and lock signals. (c) <sup>15</sup>N-chemical shifts plotted as a function of pH for peptides **1**\* (Δ, X<sub>1</sub> and X<sub>2</sub> = His), **14**\* (○, X<sub>1</sub> and X<sub>2</sub> = Ala), **15**\* (●, X<sub>1</sub> and X<sub>2</sub> = Asp), and **25**\* (■, X<sub>1</sub> and X<sub>2</sub> = His). The curves represent nonlinear least-squares fits of the data to the Henderson–Hasselbalch equation.

**Table 6.** Observed Active Site Lys ε-Amine pK<sub>a</sub> Values for Selected Peptides

peptide <sup>a</sup>	X <sub>1</sub>	X <sub>2</sub>	pK <sub>a</sub>
<b>1</b> *	His	His	9.1 ± 0.1
<b>14</b> *	Ala	Ala	9.0 ± 0.1
<b>15</b> *	Asp	Asp	10.6 ± 0.1
<b>25</b> *	His	His	9.1 ± 0.1

<sup>a</sup> The asterisk denotes AcM-protection of the active site Cys, <sup>15</sup>N enrichment of the active site Lys ε-amine, and addition of three terminal Arg residues to increase solubility. See Table 1 for full peptide sequences.

associated with pK<sub>a</sub> determination by chemical labeling methods, which can be complicated by nonspecific binding of the chemical agent to the protein or catalysis of the labeling reaction by residues other than the one of interest. Accordingly, we prepared peptides **1**\*, **14**\*, **15**\*, and **25**\* in which the active-site Lys ε-amine was selectively <sup>15</sup>N-enriched and the active-site Cys residue was alkylated with an acetamidomethyl (AcM) group to mimic the steric properties of the acylated cysteine thiolester reaction intermediate as well as to prevent oxidative disulfide formation during the course of the NMR experiments. The active-site Lys in peptide **1**\* has a pK<sub>a</sub> of 9.1, as determined by plotting the ε-amine <sup>15</sup>N NMR chemical shift versus pH and subjecting the curve to a nonlinear least-squares fit of the Henderson–Hasselbalch equation (Figures 5, S2, Table 6). This value is 1.4 units lower than the standard Lys pK<sub>a</sub> value in peptides and proteins of 10.5.<sup>15</sup> A shift in pK<sub>a</sub> of this magnitude corresponds to an approximately 30-fold increase in the ratio

(14) (a) Lodi, P. J.; Knowles, J. R. *Biochemistry* **1993**, *32*, 4338–43. (b) Zhu, L.; Kemple, M. D.; Yuan, P.; Prendergast, F. G. *Biochemistry* **1995**, *34*, 13196–202. (c) Tsilikounas, E.; Rao, T.; Gutheil, W. G.; Bachovchin, W. W. *Biochemistry* **1996**, *35*, 2437–44. (d) Zhou, Z.; Macosko, J. C.; Hughes, D. W.; Sayer, B. G.; Hawes, J.; Eppard, R. M. *Biophys. J.* **2000**, *78*, 2418–25.

of amine to ammonium (protonated) state at the pH 7.0 condition of the acyl transfer reaction, consistent with the observed 10- to 50-fold increased acylation rates. The stability and conformational homogeneity of sequence **1** over the pH range required for the  $pK_a$  titration were confirmed using circular dichroism and  $^{13}\text{C}$  NMR analyses. Circular dichroism spectra for **1** were consistent with expected  $\alpha$ -helical content and were identical at pH values of 4, 7, and 10 (Figure S1). In addition, thermal denaturation curves for **1** (carried out in the presence of 3 M guanidinium hydrochloride) yielded nearly identical  $T_m$  values of 59 °C at pH 7 and 65 °C at pH 11 (Figure S1). We further prepared a derivative of **1\***  $^{13}\text{C}$ -isotopically enriched at the C $\alpha$  position of the Leu10 residue located directly adjacent to active site Lys9 (not  $^{15}\text{N}$ -enriched in this sequence). The observed Leu10  $^{13}\text{C}\alpha$ -chemical shifts fell within the established chemical shift range for an  $\alpha$ -helical conformation<sup>16</sup> at the analyzed pH values of 5.2, 7.8, and 11.2 (Figure S3), whereas at pH 7.0 in the presence of 6.0 M guanidinium the observed Leu10  $^{13}\text{C}\alpha$ -chemical shift instead fell within the established range for random conformations<sup>17</sup> (Figure S3). Under standard reaction conditions, aminoacyl loading and transfer for **1\*** (after removal of the Ac group from the active site Cys) proceeded with rates indistinguishable from those for sequence **1**.

The  $pK_a$  of the active-site Lys in peptide **14\*** is similarly depressed to a value of 9.0 (Table 6, Figure S2), suggesting that the His residues in peptide **1\*** are not required for the observed  $pK_a$  depression and rather that proximity of the Lys side chain to the coiled-coil hydrophobic core likely causes the perturbation.<sup>5</sup> Peptide **15\***, containing acidic residues at the  $X_1$  and  $X_2$  positions, bears an active site Lys  $pK_a$  of 10.6, clearly indicating that active site residues near the aminoacyl acceptor can significantly affect its reactivity by altering the local electrostatic microenvironment. The active site Lys  $pK_a$  in peptide **25\*** is 9.1, indistinguishable from that of sequence **1\*** and suggesting a generalized  $pK_a$  perturbation for the described arrangements of residues in tetrameric coiled-coils. The observed differences in aminoacyl transfer rates for sequences **1**, **14**, and **25** thus cannot result from  $pK_a$  differences of the active site acyl acceptor, as their  $pK_a$  values are nearly identical, but the markedly poor efficiency of peptide **15** (and other sequences containing negatively charged active site residues, Table 3) most likely results from its relatively high aminoacyl-acceptor  $pK_a$  value. In contrast, positively charged or hydrophobic active site microenvironments could bring about a further depression in  $pK_a$ , consistent with the generally higher observed efficiencies of sequences containing such active sites (Table 3).

**Design of Re-engineered Peptide Sequences.** With an enhanced mechanistic understanding of the basic factors contributing to loading and transfer reactions, based on the active site  $X_1/X_2$  substitutions and  $pK_a$  titration experiments, we set out to increase the efficiency of the aminoacyl loading and transfer steps by modifying residues positioned more distant

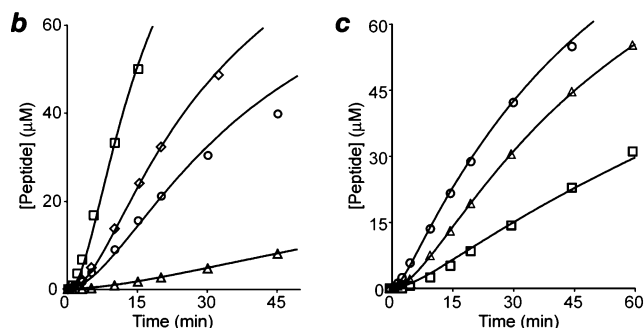
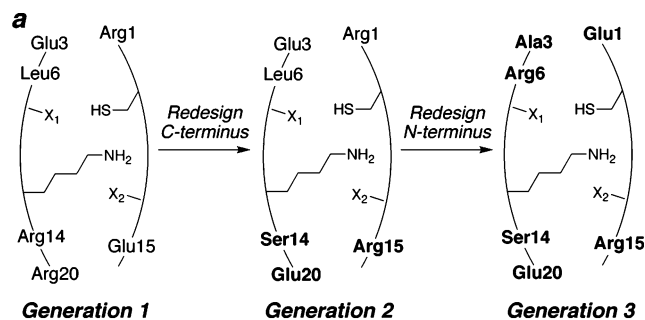


**Figure 6.** Effect of secondary sphere residues on aminoacyl transfer efficiency. (a) Schematic diagram illustrating the redesign process for secondary sphere residues leading to second and third generation peptides. See also Figure 2b for secondary sphere residue positions in the context of the coiled-coil scaffold. (b) Aminoacyl transfer product formation in time for generation 1 peptides **1** ( $\diamond$ ,  $X_1 = \text{His}$ ) and **23** ( $\triangle$ ,  $X_1 = \text{Ala}$ ) and for the corresponding generation 2 sequences **38** ( $\square$ ,  $X_1 = \text{His}$ ) and **42** ( $\circ$ ,  $X_1 = \text{Ala}$ ). (c) Aminoacyl transfer product formation in time for peptides **25** ( $\square$ , generation 1), **40** ( $\triangle$ , generation 2), and **41** ( $\circ$ , generation 3). Reaction conditions are as described in Table 2, and all curve fits shown are from reaction modeling using SIMFIT.<sup>21</sup>

from the active site. Our initial attempts at re-engineering were focused on modifications at the C-terminal side of the active site (Figure 6a) stemmed from the observations that aminoacyl loading rates ( $k_1$ ) were generally higher in sequences having the acyl donor moiety at residue 8 (peptides **8–10**, **25–30**) than at position 13 (peptides **1–7**, **11–24**). We hypothesized these effects to arise from the less sterically demanding Ser7 residue adjacent to position 8 compared to the more bulky Arg14 adjacent to position 13. Accordingly, we prepared generation-two sequences based on three C-terminal amino acid substitutions (Figure 6, Table 7). Arg14 was replaced with Ser to improve bimolecular substrate loading rates ( $k_1$ ) for sequences having the acyl donor moiety at position 13, and Glu15 and Arg20 were swapped to move the negatively charged Glu residue farther from the active site while presumably retaining the intrahelix stabilizing electrostatic salt bridge observed in the GCN4-pLI crystal structures<sup>11,12</sup> between sites 15 and 20. Three peptides (sequences **38**, **40**, and **42**) differing in active site composition were prepared based on these generation-two sequence alterations. Circular dichroism spectra indicated that the coiled-coil helical content was not significantly altered by the three C-terminal amino acid modifications (Table 1). Although aminoacyl loading rates were largely unchanged, the second-generation sequences yielded 2- to 12-fold enhanced aminoacyl transfer rates relative to the first generation peptides (Table 7, Figure 6). The observation that aminoacyl transfer in sequence **42** ( $X_2 = \text{Ala}$ ) occurs at a rate similar to that in peptide **1** suggests that the second-generation substitutions compensate for removal of His in the  $X_2$  position (Figure 6).

- (15) (a) Bundi, A.; Wuethrich, K. *Biopolymers* **1979**, *18*, 285–97. (b) Matthew, J. B.; Gurd, F. R. N.; Garcia-Moreno, B.; Flanagan, M. A.; March, K. L.; Shire, S. J. *Crit. Rev. Biochem.* **1985**, *18*, 91–197. (c) Song, J.; Laskowski, M., Jr.; Qasim, M. A.; Markley, J. L. *Biochemistry* **2003**, *42*, 2847–56.
- (16) (a) Spera, S.; Bax, A. *J. Am. Chem. Soc.* **1991**, *113*, 5490–2. (b) Holtzer, M. E.; Lovett, E. G.; D'Avignon, D. A.; Holtzer, A. *Biophys. J.* **1997**, *73*, 1031–41.
- (17) (a) Wishart, D. S.; Sykes, B. D.; Richards, F. M. *J. Mol. Biol.* **1991**, *222*, 311–33. (b) Wishart, D. S.; Sykes, B. D. *Methods Enzymol.* **1994**, *239*, 363–92.

**Table 7.** Effect of Secondary Sphere Residue Redesign on Aminoacyl Loading and Transfer Rates<sup>a</sup>

peptide	residue 8	residue 13	X <sub>1</sub>	X <sub>2</sub>	peptide length	generation	k <sub>1</sub> (10 <sup>-3</sup> s <sup>-1</sup> )	k <sub>2</sub> (10 <sup>-4</sup> s <sup>-1</sup> )
<b>1</b>	Lys	Cys	His	His	26	1	1.3	9.2
<b>38</b>	Lys	Cys	His	His	26	2	1.2	34.8
<b>39</b>	Lys	Cys	His	His	26	3	2.1	6.3
<b>25</b>	Cys	Lys	His	His	26	1	3.1	1.5
<b>40</b>	Cys	Lys	His	His	26	2	2.2	3.4
<b>41</b>	Cys	Lys	His	His	26	3	5.3	4.2
<b>23</b>	Lys	Cys	His	Ala	26	1	1.3	0.7
<b>42</b>	Lys	Cys	His	Ala	26	2	1.7	8.5
<b>5</b>	Lys	Cys	His	His	33	1	0.8	2.9
<b>43</b>	Lys	Cys	His	His	33	3	2.0	4.9
<b>8</b>	Cys	Lys	His	His	33	1	0.3	0.8
<b>44</b>	Cys	Lys	His	His	33	3	2.1	5.7

<sup>a</sup> Reaction conditions are as described in Table 2. See Table 1 for complete peptide sequences. In the 33-residue sequences, the "residue 8" and "residue 13" designations correspond to sequence positions 15 and 20 due to the seven additional N-terminal residues.

Encouraged by these results, we next focused on modifying the amino acids on the N-terminal side of the active site, again by moving negatively charged residues away from the active site while at the same time introducing a presumably stabilizing salt bridge. To this end, a potential  $i, i + 5$  electrostatic pair was incorporated by replacing Arg1 and Leu6 with Glu and Arg residues, respectively (Figure 6). Further, the Glu3 residue was substituted with an Ala to reduce overall negative charge near the active site. Circular dichroism analysis again indicated little change to the coiled-coil helical content stemming from these N-terminal substitutions (Table 1). Third-generation sequences incorporating these changes (peptides **39**, **41**, **43**, and **44**) increased aminoacyl loading rates ( $k_1$ ) by 2- to 7-fold relative to analogous earlier generation peptides (Table 7). Together with the observation that Asp at the X<sub>1</sub> or X<sub>2</sub> positions generally decreased substrate loading rates (Table 3), this finding may indicate that pK<sub>a</sub> depressions of the active site Cys (in addition to the acceptor moiety as discussed above) are important for efficient loading rates. In general, aminoacyl transfer rates ( $k_2$ ) were also improved in generation-three sequences, with the notable exception of sequence **39** (Table 7). It is unclear why transfer was nearly 6-fold reduced in this peptide relative to the second-generation sequence **38**, although the Leu6→Arg

substitution may create an electrostatic repulsion that forces the active site Lys away from the aminoacyl-donor moiety.

## Conclusions

The studies reported here show that appropriate positioning and the judicious choice of nearby amino acid residues can lead to >900-fold differences in reactivity of otherwise identical functional groups in short peptides. While the described NRPS active site models do not approach the efficiencies of natural enzymes, the observed covalent substrate binding, cooperativity among active site residues, sensitivity of the reaction rate to substitutions of active site residues, and active site pK<sub>a</sub> modulations further indicate that simple, rationally designed peptides can indeed mimic multiple features of finely tuned enzymes. Such findings will likely prove crucial in the advancement of these peptides, designed to functionally mimic NRPSs, toward a programmed peptide synthesis in which sequences of reactions are controlled by varying the relative reactivities of aminoacyl-donor and -acceptor moieties coupled with selective and sequence-dependent coiled-coil self-assembly.<sup>18</sup> It is our hope that, through such rational approaches, practical enzyme mimetics and catalysts for reactions not occurring in nature could emerge.

**Acknowledgment.** We thank Drs. Laura Pasternack and Dee-Hua Huang for assistance with <sup>15</sup>N NMR acquisition, Professor G. von Kiedrowski for the generous gift of the program SIMFIT, and the NSF for a predoctoral fellowship (L.J.L.).

**Note Added after ASAP Publication.** Due to a production error, the version of this paper published ASAP on February 16, 2007, was not the final corrected version. Additional changes were made in Tables 5–7, and the corrected version was published ASAP on February 22, 2007.

**Supporting Information Available:** Materials and methods, Figures S1–S3. This material is available free of charge via the Internet at <http://pubs.acs.org>.

JA068052X

- (18) Ashkenasy, G.; Jagasia, R.; Yadav, M.; Ghadiri, M. R. *Proc. Natl. Acad. Sci. U.S.A.* **2004**, *101*, 10872–7.
- (19) (a) O'Shea, E. K.; Klemm, J. D.; Kim, P. S.; Alber, T. *Science* **1991**, *254*, 539–44. (b) Harbury, P. B.; Kim, P. S.; Alber, T. *Nature* **1994**, *371*, 80–3.
- (20) DeLano, W. L. The PyMOL Molecular Graphics System: 2002; <http://www.pymol.org>.
- (21) Sievers, D.; von Kiedrowski, G. *Chem.—Eur. J.* **1998**, *4*, 629–41.